Electronic coupling in linear arrays of quantum cavities characterized using conductance fluctuations

Y. Takagaki and K. H. Ploog
Paul-Drude-Institut für Festkörperelektronik, Hausvogteiplatz 5-7, D-10117 Berlin, Germany
(Received 7 January 2003; revised manuscript received 25 February 2003; published 20 May 2003)

Quantum fluctuations in the conductance produced by the variation of the Fermi energy or a magnetic field are analyzed to investigate the electronic coupling in linear arrays of quantum cavities. The magnetic-field-induced fluctuations exhibit a behavior which implies an incomplete coupling among the quantum cavities. This forms striking contrast to the nearly complete coupling indicated by the energy-induced fluctuations. We examine the dependencies of these coupling coefficients estimated from the conductance fluctuations on various structural parameters. The contradiction between the two coupling coefficients is attributed to the existence of a large number of silent orbits which do not interact with the magnetic field. We also explore the consequences of the series addition of the cavities that are manifested in the underlying classical dynamics.

DOI: 10.1103/PhysRevB.67.195323 PACS number(s): 73.23.Ad, 73.63.Kv, 05.45.Pq

I. INTRODUCTION

In quantum cavities (QC's) in the ballistic transport regime, the boundary reflection of a two-dimensional electron gas (2DEG) determines the behavior of the electronic conductance. Investigations of the transport properties typically deal with either the mean conductance[1–3] or quantum fluctuations[2–8] around the mean value. The semiclassical path-integral theory[1,4,5] and random-matrix theory[2,3] predicted a weak localization effect in the mean conductance[1] based on the assumption that the classical trajectories in the cavities obey the statistical characteristics that are expected for chaotic dynamics. Experiments[9,10] and numerical simulations[7,11] confirmed the presence of the effect.

The remarkable success of the theory explaining the actual experiments tempted us to extend the semiclassical approach to make predictions for the cases in which the dynamics is regular (integrable) or mixed.[1,5,12,13] The weak localization effect was derived to exhibit a distinct magnetoconductance around zero magnetic field, which can distinguish whether the underlying classical dynamics is regular or chaotic.[1] However, numerical simulations raised a suspicion about this conclusion.[7,11,14] The reliability of the extension of the theory was checked by putting the predictions concerning the quantum fluctuations to the test. The semiclassical theory, random matrix theory, and numerical simulations agreed with each other for chaotic dynamics. However, the enhancement of the amplitude of the conductance fluctuations (CF's) reported in Ref. 7 is a clear demonstration that the standard theoretical techniques are not applicable if the dynamics is not completely chaotic.[11] Nevertheless, although refinements of the semiclassical theory[15] were necessary to satisfy ''internal consistency,''[16] the theoretical results were successfully confronted with experiments so long as chaotic QC's are concerned.

Recently, some investigations have addressed the issue of how the transport properties in a single QC are transformed when a number of QC's are connected in series. For instance, ElHassan *et al.*[17] experimentally examined the CF's in an array of three QC's, which was defined in a GaAs-(Al,Ga)As heterostructure using split-gate techniques. Their analysis led to the conclusion that the coupling among the QC's was manipulated by changing the width of the point contacts which connected the QC's.

In this paper, we numerically investigate the influences of the series connection of QC's on the statistical properties of the CF's. We compare the correlations of the CF's in single QC's and linear arrays. Strikingly different estimates are obtained for the coupling from the CF's induced by varying the Fermi energy or an external magnetic field. We provide a model that explains this behavior in terms of the probability distributions of the area that classical trajectories enclose in chaotic cavities and arrays. In the Appendix, we present the influences that the underlying classical dynamics develops as a consequence of the series addition of the cavities.

II. NUMERICAL MODEL

We examine the quantum fluctuations of the conductance in single cavities and linear arrays. The fluctuations are produced by varying either the Fermi energy E of the 2DEG in QC structures or an external magnetic field B, which is applied normal to the 2DEG. Specifically, we compare the energy and magnetic-field correlations in three QC structures: a linear array of three nominally identical QC's, an individual single QC of the array, and a single QC having a thrice larger length. The total cavity area is hence almost identical for the linear array and the long single QC. We numerically test the conjecture that, depending on the strength of the coupling among the QC's, the CF's in the array should behave similar to those in the short single QC (if the coupling is weak) or in the long single QC (if the coupling is strong).

The QC structures are simulated using a square lattice with a lattice constant a. The magnetic field is incorporated in the form of the Peierls phase factor $\exp[i(e/\hbar)\int \mathbf{A}\cdot d\mathbf{l}]$, where $\mathbf{A}$ is the vector potential. For the linear array, three rectangular cavities of identical sizes are connected in series, as illustrated in Fig. 1. An individual QC consists of N_W lattice sites in the transverse direction and N_L lattice sites in the direction of the series connection. Uniform leads and constrictions having a width corresponding to N_l lattice sites

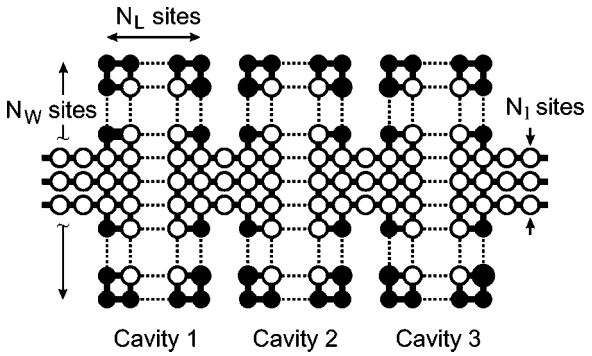

FIG. 1. Schematic of the tight-binding model to simulate a linear array consisting of three quantum cavities. Each cavity, which is referred to as the short single quantum cavity in the text, is of length $(N_L+1)a$ and width $W=(N_W+1)a$ with a being the lattice constant. The leads are of width $(N_l+1)a$. A potential disorder is introduced at the boundary lattice sites indicated by the filled circles.

are attached, unless stated otherwise, at the center of the QC's.

The validity of the semiclassical theory in dealing with open systems having regular or mixed dynamics has not been established.[18] This implies that it is necessary to realize fully chaotic dynamics in QC's for a meaningful comparison of a numerical study with analytical theories and many of experiments. We point out that a large number of previously reported numerical simulations used model QC's in which the dynamics was not completely chaotic. Due to the rectangular cavity geometry, the underlying classical dynamics would be regular in the absence of a magnetic field.[20] In order to emphasize that the results to be presented below are a generic feature in linear arrays, we enforce fully chaotic classical dynamics upon individual cavities.[21] We realize the chaotic dynamics in each QC using a short-range boundary disorder.[22] A potential disorder is introduced at the boundary lattice sites, which are indicated by the filled circles in Fig. 1. The on-site energies are modified by δE assuming a uniform distribution for δE in a range of $-d/2<\delta E<d/2$. The underlying classical dynamics is not altered by the series addition of the nearly identical cavities, see the Appendix.

The QC structures are terminated by two leads 1 and 2. We calculate the fully quantum-mechanical conductance G using the Landauer formula

$$G(E,B)=\frac{2e^2}{h}\sum_{i\in 1,j\in 2}|t_{ji}(E,B)|^2. \qquad (1)$$

The conductance is related to the transmission coefficients t_{ji} between the modes i in lead 1 and the modes j in lead 2. The transmission coefficients are calculated using the lattice Green's-function technique.[23] Throughout this paper, we assume $N_W=100$, $N_L=60$ ($=180$ for the long single QC), and $d=t$, where $t=\hbar^2/2ma^2$ is the nearest-neighbor hopping amplitude in the tight-binding lattice.

III. RESULTS AND DISCUSSION

In Fig. 2, we compare the conductance in the three QC structures. Here, E and B are normalized as $\varepsilon=E/t$ and $\beta=BW^2/\phi_0$, $W=(N_W+1)a$ is the width of the QC, and $\phi_0=h/e$ is the magnetic flux quantum. The three curves in each panel correspond to the short single QC, the linear array, and the long single QC from top to bottom, respectively. In terms of the correlation scales of the CF's, the linear array and the long single QC are similar to each other when the energy is varied, whereas the conductance of the linear array fluctuates rather in the way that of an individual QC does when the magnetic field is varied. The different degree of the coupling among the QC's in the array estimated from the CF's induced by the energy and the magnetic field is the central finding of the present paper, and we examine below this puzzling behavior in detail.

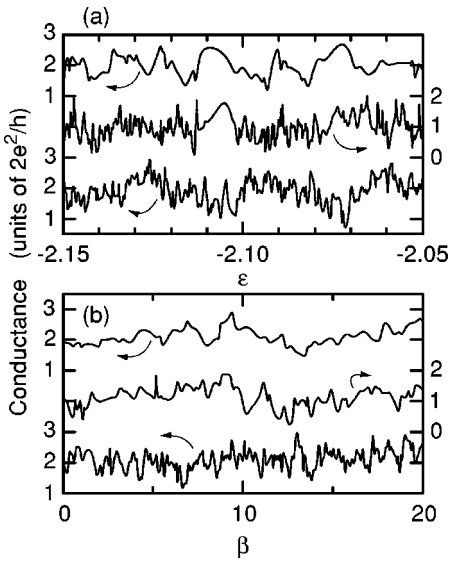

FIG. 2. Conductance of the quantum cavity structures when (a) the Fermi energy ($\varepsilon=E/t$) and (b) a magnetic field ($\beta=BW^2/\phi_0$) are varied. In (a) and (b), $\beta=0$ and $\varepsilon=-2.1$, respectively. The three curves in each panel correspond to, from top to bottom, a short single quantum cavity, an array of three short quantum cavities, and a long single quantum cavity, respectively. Curves are offset for clarity. The parameters for the short single quantum cavity are $N_W=100$, $N_L=60$, $N_l=8$, and $d=t$. The number of occupied modes N in the leads is 4.

The conductance fluctuations $\delta G=G-\langle G\rangle$, where $\langle\cdots\rangle$ denotes ensemble average, in the diffusive transport regime are typically characterized using the correlation function $\Psi_X(\Delta X)=\langle\delta G(X)\,\delta G(X+\Delta X)\rangle$, where $X=E$ or B.[24] The energy and magnetic-field scales X_c of the fluctuations are defined as $\Psi_X(X_c)=\frac{1}{2}\Psi_X(0)$. One can, in principle, carry out the same characterization for the CF's in Fig. 2. However, various transport effects modulate the mean conductance in the ballistic transport regime, making the outcome of this analysis extremely sensitive to the way the background conductance is estimated. To overcome this trouble, Jalabert *et al.*[4] further Fourier-transformed the correlation function to eliminate arbitrariness.

We employ here, instead, an alternative simple method. We have recently reported that the nearest-neighbor spacings between the peaks and dips of the CF's obey the Wigner-Dyson statistics.[8] The Wigner-Dyson distribution is anticipated, at least, in the limit of weak coupling between the QC

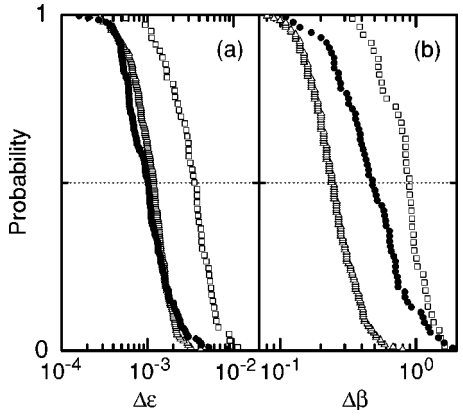

FIG. 3. Probability of the spacing between the adjacent peaks and dips of conductance fluctuations in (a) ε (energy) and (b) β (magnetic field) being larger than $\Delta\varepsilon$ and $\Delta\beta$, respectively. The probability distributions are constructed from the conductance fluctuations plotted in Fig. 2. The circles, squares, and triangles correspond to the linear array and the short and long single quantum cavities, respectively.

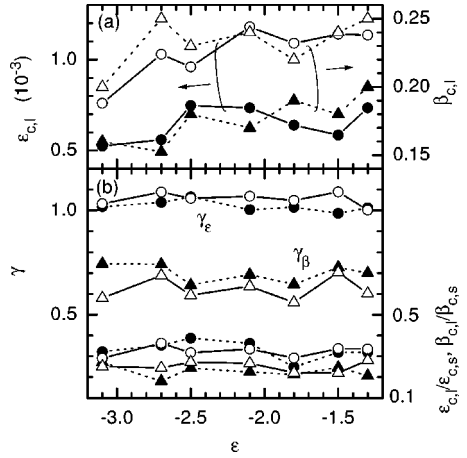

FIG. 4. (a) Dependencies of the correlation energy $\varepsilon_{c,l}$ (circles) and the correlation magnetic field $\beta_{c,l}$ (triangles) for the long single quantum cavities on the Fermi energy ε. (b) Coupling parameters γ_ε (circles) and γ_β (triangles) for the quantum cavity structures. The bottom four curves show the ratios $\varepsilon_{c,l}/\varepsilon_{c,s}$ (circles) and $\beta_{c,l}/\beta_{c,s}$ (triangles). In both (a) and (b), the filled and open symbols correspond to $N_l=4$ and 8, respectively.

and the leads as peaks and dips in the conductance due to transmission resonance take place when the Fermi energy coincides with the zero-dimensional (0D) levels in the QC. It is noteworthy that the spacings exhibit a Poisson-like distribution when the dynamics is regular.[8] The parameters that describe the Wigner-Dyson distributions can be used to quantitatively analyze the fluctuations in chaotic QC's. The advantage of this method is its practical independence on the subtraction of the background conductance. In Fig. 3, we plot the probability $P_X(\Delta X)$ of the adjacent peaks and dips being larger than ΔX. We further simplify our analysis by defining the correlation energy ε_c and the correlation magnetic field β_c as $P_\varepsilon(\varepsilon_c)=P_\beta(\beta_c)=\frac{1}{2}$. This definition enables us to determine the correlation scales unambiguously irrespective of the role of the time-reversal symmetry on $P_X(\Delta X)$.[8]

In Fig. 4(a), we show ε_c and β_c for the long single QC's as a function of the Fermi energy for two lead widths $N_l=4$ (filled symbols) and 8 (open symbols). The conductance fluctuations become wider in both ε and β when the Fermi energy is raised. The dependencies of $\varepsilon_{c,l}$ and $\beta_{c,l}$ on the Fermi energy and N_l are notably similar. ElHassan *et al.*[17] estimated the coupling among the QC's in an array by comparing the correlation scale in the array with that in a single QC. We, therefore, plot in Fig. 4(b) the coupling parameter

$$\gamma_X=\frac{X_{c,s}-X_{c,a}}{X_{c,s}-X_{c,l}}, \tag{2}$$

where $X_{c,a}$, $X_{c,s}$, and $X_{c,l}$ are the correlation scales for the linear array and the short and long single QC's, respectively. The coupling parameters are nearly independent of the Fermi energy in spite of the energy dependence of ε_c and β_c, plausibly because the cavity geometry is unchanged.

We find $\gamma_\varepsilon\approx 1$, i.e., the energy correlation in an array is almost identical to that in a single QC having an identical total cavity area. In the diffusive transport regime, the same behavior has been observed for the magnetic-field-induced CF's.[25] However, the value of $0.5\sim 0.8$ for γ_β in Fig. 4(b) is an apparent violation of this naive expectation when the transport is ballistic. The coupling appears to be weaker for wider leads, which we investigate further below. The size scaling for the energy-induced CF's and the nonscaling for the magnetic-field-induced CF's also occur between the short and long single QC's. The curves in the bottom part of Fig. 4(b) show $\varepsilon_{c,l}/\varepsilon_{c,s}$ and $\beta_{c,l}/\beta_{c,s}$. The energy correlation yields the expected value of $\frac{1}{3}$, whereas the ratio is only about 0.23 for the magnetic-field correlation. Therefore, the correlation magnetic field does not correspond to an addition of a magnetic flux quantum into the cavity area.[24] In other words, the effective cavity area does not scale with the geometrical cavity area. The energy scale of CF's is proportional to $\Delta N/2\pi$, where Δ is the mean resonance spacing and N is the number of modes in the leads.[3,26] As Δ is in proportion to the area S of the QC, $\varepsilon_{c,l}/\varepsilon_{c,s}=\frac{1}{3}$ is expected, as observed in the present numerical simulation. The magnetic-field correlation scale was estimated to vary with S as $\propto S^{5/4}$.[27] According to this relation, $\beta_{c,l}/\beta_{c,s}=0.25$ is expected, thus explaining the numerical result.

The dependencies of the characteristics of the CF's on the lead width are displayed in Figs. 5(a) and 5(b). With increasing N_l, ε_c and β_c increase roughly linearly. Fine structures in the CF's are smeared for larger N_l as the level broadening resulting from an opening to the external leads is greater for the wider leads. Here again, γ_ε remains nearly unchanged at ~ 1. Although one may anticipate widening the leads to enhance the coupling between the cavities, γ_β, on the contrary, tends to decrease with increasing N_l.

The fluctuations in the conductance of the ballistic QC's are, in principle, associated with the quasi-0D confined states. In regular QC's, the CF's bear an appearance of consisting of narrow peaks and dips due to transmission resonances.[8] These sharp features are broadened when the

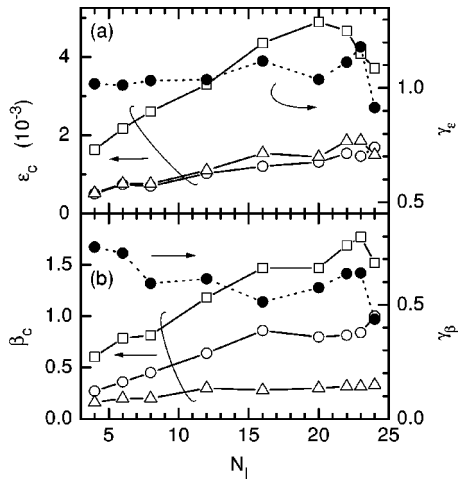

FIG. 5. Variation of the correlation properties of conductance fluctuations when the lead width N_l is varied for the (a) energy- and (b) magnetic-field-induced fluctuations. The filled circles show the coupling parameters γ. The correlation energy ε_c and the correlation magnetic field β_c are shown by the open symbols. The circles, squares, and triangles correspond to the linear array and the short and long single quantum cavities, respectively. In (a) and (b), $\beta=0$ and $\varepsilon=-3.1$, respectively.

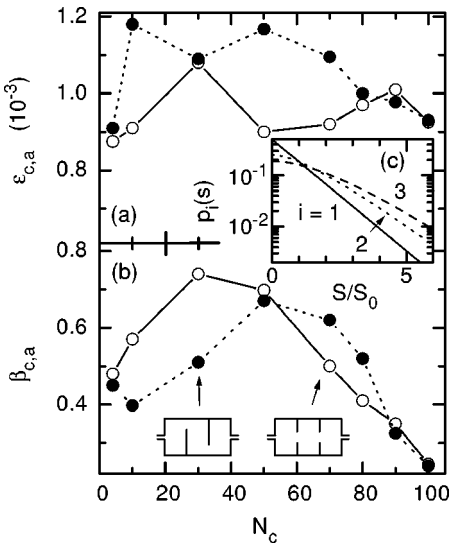

FIG. 6. Dependencies of the correlation scales (a) $\varepsilon_{c,a}$ and (b) $\beta_{c,a}$ in the arrays on the width of the constrictions N_c that connect the quantum cavities. The two configurations of the constrictions are illustrated in the insets of (b). In (a) and (b), $\beta=0$ and $\varepsilon=-3.1$, respectively. The width of the leads is $N_l=10$. Three modes are occupied in the leads. (c) Probability densities $p_i(S)$ for the area S ($-\infty<S<\infty$) enclosed by classical trajectories given by Eqs. (3)–(5). The solid, dashed, and dotted lines correspond to a single cavity, $i=1$, a linear array of two cavities, $i=2$, and a linear array of three cavities, $i=3$, respectively.

underlying classical dynamics is made chaotic. The instability of the classical trajectories in the chaotic cavities allows electrons to leave the cavities rather quickly (sooner than a quasibound state is firmly built up), resulting in an effective enhancement of the coupling of the quasi-0D state to the leads, i.e., the softening of the CF features.

If the broadening of the energy levels due to the coupling to the leads is less than the typical energy separations, the energy level splitting as a consequence of the series connection of the QC's is entirely reflected in the CF's.[8] On the one hand, the nearest-neighbor energy level separation δE in chaotic QC's obey the Wigner-Dyson statistics, i.e., the probability for $\delta E\rightarrow 0$ is infinitesimally small.[28] On the other hand, the energy level separation among the split states produced by the series connection in the array is proportional to the intercavity coupling strength. The variation of ε_c with the total cavity area in Figs. 4 and 5 indicates that the intercavity coupling in our model is always strong, so that Wigner-Dyson statistics for δE is established also in the linear arrays. In this situation, the series connection results in a complete multiplication of the energy levels and the mean energy level spacing changes in accordance with the QC sizes.

The fact that γ_β is significantly less than unity suggests that there exist a large number of classical orbits which enclose nil nominal area. These orbits do not contribute to the CF's when the magnetic field is varied. For chaotic dynamics, the probability $p_1(S)dS$ for the classical trajectories to enclose an area in the range S and $S+dS$ decays exponentially with S. Therefore, the presence of the "silent" orbits is inherently expected.

We propose the following model to explain the behavior $\gamma_\beta<1$. Let us first consider, for simplicity, the case of a series addition of two cavities. Suppose that the probability density for a single cavity is given by

$$p_1(S)=\frac{1}{2S_0}e^{-|S|/S_0}, \tag{3}$$

where $-\infty<S<\infty$. In the linear array of two cavities, the total enclosed area is given by either adding or subtracting the area enclosed in each cavity. The probability density in the linear array is hence derived to be

$$p_2(S)=\int_{-\infty}^{\infty}p_1(S-t)p_1(t)dt=\frac{|S|+S_0}{4S_0^2}e^{-|S|/S_0}. \tag{4}$$

Similarly, we find for an array of three cavities

$$p_3(S)=\frac{S^2+3S_0|S|+3S_0^2}{16S_0^3}e^{-|S|/S_0}. \tag{5}$$

We plot $p_1(S)$, $p_2(S)$, and $p_3(S)$ in Fig. 6(c). The expectation value of the enclosed area is $\langle S\rangle_i=\int_{-\infty}^{\infty}|S|p_i(S)dS=S_0$, $\frac{3}{2}S_0$, and $\frac{15}{8}S_0$ when the number i of the QC's is 1, 2, and 3, respectively. The effective cavity area thus increases sublinearly with i. The corresponding value of γ_β is ≈ 0.6 (0.7) for $\beta_{c,l}/\beta_{c,s}=0.23$ ($\frac{1}{3}$), in good agreement with the numerical results.

The above argument assumes uniform coupling between the trajectories in each cavity. In reality, this is not likely the case. The importance of the injection properties of electrons from the lead into the QC is manifested in Figs. 6(a) and 6(b).[29] In all the preceding simulations, the leads and the constrictions were positioned at the center of the QC's, allowing a direct path between the leads through the interior of

the QC's. The direct coupling is disrupted for the filled circles in Figs. 6(a) and 6(b) by arranging the constrictions at the alternate sides of the QC's, as illustrated in the left-hand-side inset of Fig. 6(b).[7] Here, the width of the constrictions $(N_c+1)a$ is varied while keeping the width of the external leads fixed $(N_l=10)$. For comparison, the open circles show $\varepsilon_{c,a}$ and $\beta_{c,a}$ when the constrictions are placed at the center of the QC's, as in Fig. 5. The width of the external leads is, however, set to be $N_l=10$, see the right-hand-side inset of Fig. 6(b). The coupling in terms of the energy-induced CF's remains almost perfect, and thus $\varepsilon_{c,a}$ is independent of the configuration and the width of the constrictions. In contrast, $\beta_{c,a}$ exhibits an appreciable dependence on the constriction position, unless the constrictions become too wide, i.e., the constriction width is larger than $W/2$. It is noteworthy that, in the regime where the position of the constrictions plays a role, $\beta_{c,a}$ increases when the constrictions are widened, i.e., the effective cavity area decreases on the contrary to the anticipation. The opposite dependence, which is interpreted to mean a stronger coupling for wider constrictions, takes place when the position of the constrictions is irrelevant. (Notice that the case of $N_c=100$ is equivalent to the long single QC, and so the latter behavior is inevitable.)

Finally, let us briefly remark on the experiment by ElHassan *et al.*[17] A transition of conductance fluctuations in linear arrays between multiple and single QC behaviors was observed when the bias applied to the split gates was varied. Unlike the case of the strong coupling in our simulations, the competition between the energy level splitting and the level broadening due to the opening to the environment explicitly takes place if the coupling between the QC's is weak. We speculate that this was the situation in the experiment. Our simulations were carried out for zero temperature. The energy levels are additionally broadened by the finite lifetime of electrons in the QC's in real devices.[26] The coupling in the array cannot avoid the influence of the finite temperature when the QC sizes are comparable to the thermal length or the phase coherence length.

IV. CONCLUSION

We have investigated the electronic coupling among chaotic quantum cavities when they are connected in series. We have quantified the degree of the coupling by means of the statistics of the spacings between the adjacent peaks and dips of conductance fluctuations. When the fluctuations are induced by varying the Fermi energy, the linear array is equivalent to a single quantum cavity having the same total cavity area. For magnetic-field-induced fluctuations, the effective cavity area in the linear array is in-between the effective areas of an individual quantum cavity of the array and a single quantum cavity having the same total geometrical area. This seemingly inconsistent appearance of the coupling strength originates from the fact that the probability distributions for the nearest-neighbor energy level separation and the area enclosed by classical trajectories follow different functional forms.

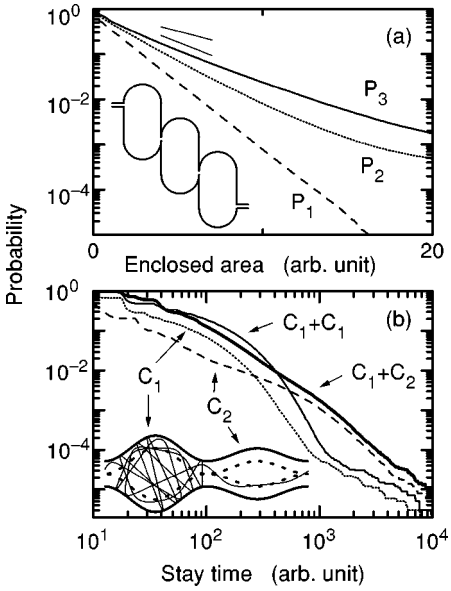

FIG. 7. (a) Probability $P_i(S)$ of the area enclosed by classical trajectories being larger than S $(\geqslant 0)$. The number i of stadium-shaped cavities is 1, 2, and 3 for the dashed, dotted, and solid lines, respectively. The thin solid lines indicate the slopes when the decay constant for the exponential behavior is twice or thrice larger than that for $i=1$. The inset illustrates the array of stadium-shaped cavities with $i=3$. (b) Probability of electrons remaining in the soft-wall cavities longer than the stay time. The dashed and dotted lines show the probabilities in the single cavities C_1 and C_2, respectively. Two cavities are connected in series for the thin (two identical cavities C_1) and thick (C_1 and C_2) solid lines. The inset illustrates the array consisting of cavities C_1 and C_2. The thick solid and dashed lines indicate the cavity boundary at the Fermi energy and the inner boundary of the soft-wall potential, respectively. The thin solid line shows an example of classical trajectories.

ACKNOWLEDGMENTS

This work was supported in part by the Deutsche Forschungsgemeinschaft and by the NEDO collaboration program.

APPENDIX: CLASSICAL DYNAMICS IN CAVITY ARRAYS

This appendix is devoted to investigate the evolution of the underlying classical dynamics when a number of cavities are added in series. It is not practical to use the short-range boundary disorder to generate chaotic dynamics in a classical model. Here, we rather employ stadium geometry for the cavities to serve the purpose. The inset of Fig. 7(a) displays an array of three stadium cavities, which are defined by hard-wall potentials. The three curves in Fig. 7(a) show the probability $P_i(S)$ for the area enclosed by classical trajectories being larger than S $(\geqslant 0)$. The number i of the stadiums is increased from 1 to 3 for the dashed, dotted, and solid lines. The exponential decay of the probability P_1 for the single cavity evidences chaotic dynamics. When a number of cavities are added in series, the corresponding probability distributions deviate from the exponential decay for large

enclosed areas. If we approximate the initial decay of $P_i(S)$ at small S by an exponential behavior, the enhancement factor of the decay constant in the arrays in comparison to that in the single cavity is found to be less than i. (The thin solid lines indicate the slopes when the decay constant in the single cavity is multiplied by 2 or 3.) Therefore, although the functional form of $P_i(S)$ in Fig. 7(a) is different from the analytical expressions, Eqs. (4) and (5), the sublinear increase of the enclosed area with i is confirmed. The expectation value of the enclosed area in the array is by factors of 1.6 and 2.1 larger than that in the single cavity for $i=2$ and 3, respectively.

In the remainder, we turn our attention to the classical dynamics in soft-wall cavities. The model geometry of the cavities is illustrated in the inset of Fig. 7(b). We consider two dissimilar cavities, which we refer to as C_1 and C_2. (They are connected in series in the inset.) The cavity boundary at the Fermi level, which is shown by the thick solid lines, is defined by two cosine curves. Parabolic potentials are assumed in the vicinity of the boundary between the solid and dashed lines.[5,19] For the spatially varying potential $U(x,y)$, the electrons are, upon approaching the boundary, gradually deflected by a force $\mathbf{F}(x,y)=-\nabla U(x,y)$. We calculate the classical trajectories by solving Newton's equation numerically using a predictor-corrector method

$$\mathbf{x}_{i+1}=\mathbf{x}_i+\mathbf{v}_i\Delta T+\frac{\mathbf{F}(\mathbf{x}_i)}{2m}(\Delta T)^2, \tag{A1}$$

$$\mathbf{v}_{i+1}=\mathbf{v}_i+\frac{\mathbf{F}(\mathbf{x}_i)+\mathbf{F}(\mathbf{x}_{i+1})}{2m}\Delta T, \tag{A2}$$

where $\mathbf{x}_i=(x_i,y_i)$ and $\mathbf{v}_i$ are the position and the velocity of an electron at the ith time step of period ΔT.

Generally speaking, the soft-wall confinement leads to mixed dynamics, and so the probability distributions are given by power laws. In the case of Fig. 7(b), however, the probability of electrons remaining in the cavity longer than the stay time does not exactly exhibit the power-law decay as, for better presentation of the effects of the series addition of the cavities, the parameters were chosen such that the soft-wall confinement is insufficient to realize complete mixed dynamics. The probability distribution when two identical cavities are added in series, denoted C_1+C_1 in Fig. 7(b), can be regarded as given by doubling the stay time, i.e., the series addition does not alter the fundamental properties of the underlying classical dynamics. When the two dissimilar cavities are added in series, denoted C_1+C_2, the probability distribution is given as a superposition of that in each cavity, resulting in, in this particular case, a power-law decay over a wider range of the stay time. Therefore, the fractal properties of CF's in soft-wall cavities are expected to be modified by adding dissimilar cavities.

In the above-presented simulations based on the billiard model, classical particles are injected from the lead into the cavity assuming smooth positional and angular distributions. These distributions, however, do not necessarily remain regular when the particles leave the cavity. This gives rise to a possibility of having fundamentally different probability distributions between a single cavity and an array if the injection distributions from a cavity in the array into adjacent cavities are irregular, for instance, with hierarchical features typically observed for mixed dynamics. Nevertheless, the fact that summing up the probability distribution in each cavity can account for the probability distribution in the array suggests that the role of the particle injection is minor. The assumption of the uniform coupling in deriving Eqs. (4) and (5) is hence justified.

[1] H. U. Baranger, R. A. Jalabert, and A. D. Stone, Phys. Rev. Lett. **70**, 3876 (1993).

[2] C. W. J. Beenakker, Rev. Mod. Phys. **69**, 731 (1997).

[3] Y. Alhassid, Rev. Mod. Phys. **72**, 895 (2000).

[4] R. A. Jalabert, H. U. Baranger, and A. D. Stone, Phys. Rev. Lett. **65**, 2442 (1990).

[5] R. Ketzmerick, Phys. Rev. B **54**, 10841 (1996).

[6] Y. Takagaki and K. H. Ploog, Phys. Rev. B **61**, 4457 (2000).

[7] Y. Takagaki and K. H. Ploog, Phys. Rev. B **63**, 125311 (2001).

[8] Y. Takagaki and K. H. Ploog, Phys. Rev. B **64**, 245336 (2001).

[9] C. M. Markus, A. J. Rimberg, R. M. Westervelt, P. F. Hopkins, and A. C. Gossard, Phys. Rev. Lett. **69**, 506 (1992).

[10] A. M. Chang, H. U. Baranger, L. N. Pfeiffer, and K. W. West, Phys. Rev. Lett. **73**, 2111 (1994).

[11] Y. Takagaki and K. H. Ploog, in *Proceedings of the 28th International Symposium on Compound Semiconductors*, Tokyo, 2001 (IOP Publishing, Bristol, 2002), p. 357.

[12] B. Huckestein, R. Ketzmerick, and C. H. Lewenkopf, Phys. Rev. Lett. **84**, 5504 (2000).

[13] A. Bäcker, A. Manze, B. Huckestein, and R. Ketzmerick, Phys. Rev. E **66**, 016211 (2002).

[14] R. Akis, D. K. Ferry, J. P. Bird, and D. Vasileska, Phys. Rev. B **60**, 2680 (1999).

[15] K. Richter and M. Sieber, Phys. Rev. Lett. **89**, 206801 (2002).

[16] R. O. Vallejos and C. H. Lewenkopf, J. Phys. A **34**, 2713 (2001).

[17] M. ElHassan, J. P. Bird, A. Shailos, C. Prasad, R. Akis, D. K. Ferry, Y. Takagaki, L.-H. Lin, N. Aoki, Y. Ochiai, K. Ishibashi, and Y. Aoyagi, Phys. Rev. B **64**, 085325 (2001).

[18] The theory regarding the fractal CF's (Ref. 5) has to be taken cautiously as they are associated with mixed dynamics. All classical trajectories are unstable in chaotic dynamics, whereas the hierarchical mixture of a chaotic sea and regular orbits in the phase space for mixed dynamics gives rise to the presence of stable orbits. Treating the exponential term that contains the classical action in the semiclassical path-integral approach as a random complex number (Refs. 1,4,5) may be invalidated if certain trajectories are favored by the cavity dynamics (Ref. 11). In Ref. 19, the fractal dimension was shown to disagree considerably between classical and quantum-mechanical simulations, although the two simulations agreed well with respect to the scarlike features originating from the stable orbits. Mixed dynamics may necessitate a reexamination of the theory that links the fractal dimension to the power-law exponent of the probability distributions (Ref. 5).

[19] Y. Takagaki and K. H. Ploog, Phys. Rev. E **62**, 4804 (2000).

[20] Y. Takagaki, M. ElHassan, A. Shailos, C. Prasad, J. P. Bird, D. K. Ferry, K. H. Ploog, L.-H. Lin, N. Aoki, and Y. Ochiai, Phys. Rev. B **62**, 10255 (2000).

[21] We note, however, that no specific dependencies of the coupling among the QC's on the underlying classical dynamics are observed in our simulations.

[22] E. Cuevas, E. Louis, and J. A. Vergés, Phys. Rev. Lett. **77**, 1970 (1996).

[23] T. Ando, Phys. Rev. B **44**, 8017 (1991).

[24] P. A. Lee, A. D. Stone, and H. Fukuyama, Phys. Rev. B **35**, 1039 (1987).

[25] A. D. Benoit, C. P. Umbach, R. B. Laibowitz, and R. A. Webb, Phys. Rev. Lett. **58**, 2343 (1987); W. J. Skocpol, P. M. Mankiewich, R. E. Howard, L. D. Jackel, D. M. Tennant, and A. D. Stone, *ibid.* **58**, 2347 (1987).

[26] E. R. P. Alves and C. H. Lewenkopf, Phys. Rev. Lett. **88**, 256805 (2002).

[27] Z. Pluhar, H. A. Weidenmüller, J. A. Zuk, C. H. Lewenkopf, and F. J. Wegner, Ann. Phys. (N.Y.) **243**, 1 (1995).

[28] E. R. Mucciolo, R. B. Capaz, B. L. Altshuler, and J. D. Joannopoulos, Phys. Rev. B **50**, 8245 (1994).

[29] Y. Takagaki and D. K. Ferry, Phys. Rev. B **45**, 13 494 (1992).